Energy Advances

ROYAL SOCIETY OF CHEMISTRY

PAPER

View Article Online
View Journal | View Issue

Cite this: *Energy Adv.*, 2024, 3, 829

Bimetallic and plasmonic Ag and Cu integrated TiO_2 thin films for enhanced solar hydrogen production in direct sunlight†

Sunesh S. Mani,[a] Sivaraj Rajendran,[a] Pushkaran S. Arun,[a] Aparna Vijaykumar,[a] Thomas Mathew*[a] and Chinnakonda S. Gopinath*[bc]

Plasmonic metal nanoparticle-integrated mesoporous TiO_2 nanocomposites (Ag/TiO_2, Cu/TiO_2 and Ag–Cu/TiO_2), prepared by a simple chemical reduction method, have been demonstrated to show superior activity in thin-film form for solar H_2 generation in sunlight. Integration of Ag + Cu on TiO_2 significantly enhances the solar H_2 production due to the combined SPR effect of both metal species and the possible synergistic interaction among Cu + Ag in Ag–Cu/TiO_2. TiAgCu-1 (0.75 wt% Ag and 0.25 wt% Cu on TiO_2) showed the highest H_2 yield of 6.67 mmol h^{-1} g^{-1} and it is 43 times higher than that of bare TiO_2. The thin-film form of TiAgCu-1 shows 5 times higher solar H_2 production than its powder counterpart. 1 wt% of Ag or Cu on TiO_2 shows a H_2 yield of 4.6 or 2 mmol h^{-1} g^{-1}, respectively, which underscores the importance of combined or synergistic effects. The increase in solar H_2 generation in Ag–Cu/TiO_2 is attributed to factors such as the SPR effect of Cu and Ag, and strong interaction between Ag and Cu. The high photocatalytic efficiency of the TiAgCu-1 thin film is attributed to the large dispersion of metallic species with relatively high Ag/Cu surface atomic ratio, enhanced light absorption, a heterogeneous distribution of Ag and Cu species, and high double layer capacitance. The inter particle mesoporous network increases the interfacial charge transfer and reduces the mass transfer limitations. The plausible photocatalytic reaction mechanism could involve the combination of direct electron transfer from metal (Cu/Ag) to TiO_2 as well as the significant field effect due to the Ag–Cu alloy, which is expected to increase the electron excitation locally.

Received 27th January 2024,
Accepted 7th March 2024

DOI: 10.1039/d4ya00056k

rsc.li/energy-advances

Introduction

The development of electronically integrated photocatalytic materials that could efficiently catalyze water splitting by utilizing solar energy to produce clean H_2 is of great importance, especially in view of the world wide focus on the use of renewable energy and the increasing concern regarding environmental issues.[1–5] Ever since the potential of TiO_2 in photocatalytic applications was realized by Fujishima and Honda in 1972, there has been a perpetual interest in the design and fabrication of visible light-driven photocatalytic materials for practical applications.[5–7] Integration with metal nanoparticles, which also exhibit surface plasmon resonance (SPR), is one of the effective strategies for enhancing the visible light harvesting capability and photocatalytic performance of TiO_2 by suppressing the electron–hole recombination.[8] Recently, we have reported the synthesis of Ag/TiO_2 and M-Au/TiO_2 (M = Ag, Pd and Pt) nanocomposites with accessible mesopores and demonstrated the high potential of this material for solar H_2 evolution.[2] The SPR effect shown by Ag nanoparticles enhances the absorption of visible light.[9–11] However, it is more desirable that the activity of Ag/TiO_2 can be improved in a way by adding a synergistically interacting and catalytically active metal, such as Cu into it; indeed this is expected to make it a bimetal/alloy nanoparticle system,[12] which would improve the charge separation and also provide more active sites for efficient H_2 production.[5,13] Among the 3d transition metal series, Cu is one of the preferred choices due to its SPR nature, co-catalytic ability, and fast electron transfer rate.[14] The combined effect of Cu and Ag in enhancing the photocatalytic activity with Ag–Cu/TiO_2 photocatalysts by taking advantage of the co-catalytic as well as SPR effect of both Ag and Cu has not been reported in the literature.[13] Incorporation of Cu in Ag/TiO_2 brings changes in the physico-chemical characteristics, such as

[a] *Department of Chemistry, St. John's College, Anchal, Kerala 691308, India. E-mail: thomasmathew@stjohns.ac.in*
[b] *Catalysis and Inorganic Chemistry Division, CSIR – National Chemical Laboratory, Dr HomiBhabha Road, Pune 411 008, India. E-mail: cs.gopinath@ncl.res.in*
[c] *Academy of Scientific and Innovative Research (AcSIR), Ghaziabad 201002, India*

† Electronic supplementary information (ESI) available: FESEM, HRTEM-EDS, Ag/Cu atomic ratio, impedance parameters, XPS binding energy values, and H_2 rate comparison. See DOI: https://doi.org/10.1039/d4ya00056k

the availability of two metals on the TiO_2 surface, and possible redox interactions in close-proximity can minimize the electron–hole recombination rate.[15,16]

In the present manuscript, we report the synthesis of metal–TiO_2 mesoporous nanocomposites (Ag/TiO_2, Cu/TiO_2 and Ag–Cu/TiO_2) by integrating metal nanoparticles on mesoporous TiO_2 through a simple chemical reduction method. The photocatalytic H_2 production activity of these materials in thin-film form was evaluated in detail and demonstrated the superior catalytic performance of bimetallic Ag–Cu/TiO_2 over single metal (Ag or Cu)/TiO_2 nanocomposites. Although the photocatalytic H_2 evolution activity of the bimetallic Ag–Cu/TiO_2 photocatalytic material is reported in the literature,[13,15,17] to the best of our knowledge, Ag–Cu/TiO_2 nanocomposites fabricated in thin-film form with the highest solar hydrogen evolution in direct sunlight and a detailed structure–activity relation are reported for the first time in the present manuscript.

Experimental

Synthesis of mesoporous TiO_2, Cu/TiO_2 and Ag–Cu/TiO_2 nanocomposites

The chemicals used for the synthesis of mesoporous TiO_2, Cu/TiO_2, Ag/TiO_2 and Ag–Cu/TiO_2 nanocomposites include titanium tetra-isopropoxide (TTIP) (Sigma Aldrich), silver nitrate (Sigma Aldrich), copper nitrate tri hydrate (Loba-Chimie), polyethylene oxide (PEO) (average molecular weight: 100 000, Sigma Aldrich), hydrazine hydrate (Loba-Chemie), formamide (Loba-Chemie), nitric acid (Loba-Chemie), ammonia (28–30%) (Loba-Chemie), iso-propyl alcohol (Loba-Chemie), and *n*-hexane (Loba-Chemie). All the chemicals were used as supplied, without any further purification.

The synthesis of mesoporous TiO_2 nanoparticles was accomplished *via* a sol–gel technique as previously reported by our group.[2] Briefly, the synthesis of TiO_2 nanoparticles was carried out in aqueous medium using a mixture of TTIP as a Ti source, acetic acid as a peptizing agent, and PEO as a surfactant. Formamide and NH_3 were used for adjusting the pH to get titania gel followed by a sequence of solvent exchange processes using isopropanol and *n*-hexane. The solvent-free gel was then allowed to dry at 60 °C for 48 h and finally calcined at 500 °C at a heating rate of 2 °C min^{-1}. Cu integrated TiO_2 nanocomposites with different Cu content (0.5, 1 and 5 wt%) were prepared by using hydrazine hydrate as a reducing agent. Briefly, the required amount of $Cu(NO_3)_2{\cdot}3H_2O$ was dissolved in 95 mL water and the calculated amount of mesoporous TiO_2 nanoparticles was introduced into this solution. Chemical reduction of Cu^{2+} ions on TiO_2 was carried out by adding about 5 mL hydrazine hydrate–water mixture (containing 0.9 g hydrazine hydrate) drop-wise under vigorous stirring. During the addition, a change in the colour of the suspension from white to reddish brown was observed, which indicates the reduction of Cu^{2+} to Cu^0. The entire mixture was then kept for 2 h under stirring, followed by drying at 60 °C for 12 h and calcination at 300 °C for 3 h. The Cu/TiO_2 nanocomposites thus prepared in the present study are designated as TiCu-0.5 (0.5 wt% Cu on TiO_2), TiCu-1 (1 wt% Cu on TiO_2), and TiCu-5 (5 wt% Cu on TiO_2), hereafter. Ag–Cu/TiO_2 nanocomposites with different wt% of Ag and Cu were prepared by a similar procedure using the respective metal ion sources $Cu(NO_3)_2{\cdot}3H_2O$ and $AgNO_3$ in the required proportions and the samples are designated as TiAgCu-1 (0.75 wt% Ag and 0.25 wt% Cu on TiO_2), TiAgCu-2 (0. 5 wt% Ag and 0.5 wt% Cu on TiO_2), and TiAgCu-3 (0.25 wt% Ag and 0.75 wt% Cu on TiO_2). For comparison, 1 wt% Ag/TiO_2 (TiAg-1) was also prepared, as described above, with the required amount of $AgNO_3$.

Material characterization

X-ray powder diffraction (XRD) analysis was carried out on a Bruker D8 Avance diffractometer using Cu Kα radiation (λ = 1.540598 Å) and a Ni-filter. The data were collected with a step size of 0.02° at a scan rate of 0.5° min^{-1}. Transmission electron microscopy (TEM) images were recorded using a Jeol/JEM 2100 electron microscope operating at 200 kV and the images were analysed using Image J software. HRTEM EDS mapping was conducted on a JEOL JEM F-200 HTEM instrument operating at 200 kV equipped with EDS; since the catalysts contain Cu, a gold-coated grid was employed to measure the Cu and Ag content. UV-visible spectral measurement was performed using an Agilent spectrophotometer (Cary 5000) under absorption mode for the powder sample with spectral-grade $BaSO_4$ as the reference material. X-ray photoelectron spectra (XPS) were acquired from a Thermo Scientific ESCALAB Xi^+ kα spectrometer using a monochromatic Al Kα anode (1486.6 eV) as the X-ray source. Static charge correction was made with reference to the C 1s peak (284.6 eV).

Photoelectrochemical measurements

Transient photocurrent measurements were performed with an electrochemical workstation (CHI 6041E). The catalyst sample coated as a thin film on a fluorine-doped tin oxide (FTO) glass plate to 1.0 cm^2 area was used as the electrode for measurements. The electrochemical experiments were carried out in a 0.5 M Na_2SO_4 (pH = 7.5) electrolyte solution at a potential of 1.23 V (*vs.* NHE). A LED lamp (50 W) was used as the light source. A three-electrode system was used for electrochemical measurement, which included Pt wire, Ag/AgCl, and the electrode material prepared on an FTO plate as the counter electrode, the reference electrode, and working electrode, respectively. The electrochemical impedance was measured using a similar experimental setup.

Photocatalytic activity measurements

The photocatalytic hydrogen production activity of mesoporous TiO_2, Cu/TiO_2 and the Ag–Cu/TiO_2 nanocomposites in both powder and thin film forms were evaluated under direct sunlight between 10 am and 4 pm during April/May months in our laboratory premises at Anchal, Kerala, India using aqueous methanol 25% (v/v) solution.[2] An optimized amount of 1 mg of the photocatalyst was dispersed in 1 mL ethanol and the suspension obtained after sonication of it was then drop cast

on a glass substrate of dimensions 1.25 × 3.75 cm^2 to make a thin film of the photocatalyst. The dried film was then carefully kept inside in a 70 mL capacity quartz round bottom flask (RBF) containing aqueous methanol solution and closed with an air tight septum. The RBF was de-aerated by purging N_2 gas for 30 min before the activity measurement. The activity of the catalyst was also tested with 1 mg of powder sample under similar conditions. The powder material was made in suspension form by sonication for 15 min to obtain a uniform dispersion of the catalyst before the photocatalytic measurements. The activity of the powder or thin film catalyst was investigated under stirring conditions in direct sunlight. The hydrogen evolution from different catalysts was analyzed periodically with a PerkinElmer Clarus 590 gas chromatograph (GC) equipped with a thermal conductivity detector at 200 °C. The apparent quantum yield (AQY) of solar hydrogen for all the catalysts was calculated according to the formula given in eqn (1).[18,19]

$$\text{AQY}\ (\%) = \frac{2 \times \text{number of } H_2 \text{ molecules}}{\text{Number of incident photons}} \times 100 \qquad (1)$$

For the above calculation, the assumptions are 9% photons from the wavelength range 370 to 500 nm are incident, which corresponds to 8.3 × 10^{18} photons per second.

Results and discussion

Synthesis aspects and textural properties of the photocatalysts

The various steps involved in metal integration with mesoporous TiO_2 are provided in Scheme 1 by illustrating the preparation of mesoporous Ag–Cu/TiO_2. All nanocomposites (Ag/TiO_2, Cu/TiO_2 and Ag–Cu/TiO_2) in the present study were prepared by a chemical reduction method using hydrazine as the reducing agent. $Cu(NO_3)_2{\cdot}3H_2O$ and $AgNO_3$ in required proportions were used as the Cu and Ag source, respectively. During the reduction process, Cu^{2+} and Ag^+ were reduced to Cu^0 and Ag^0, respectively. Mesoporous TiO_2 with high surface area (98 m^2 g^{-1}) was employed for post-modification, as reported earlier.[2a] The interconnected mesoporous TiO_2 network with significant pore volume (0.2 mL g^{-1}) provides a large number of unsaturated as well as oxygen vacancy sites with high electron density are primarily the sites for Cu^{2+} and Ag^+ ions to adsorb followed by reductive integration with titania in the presence of hydrazine. Thereby a high dispersion and integration of Cu and Ag on TiO_2 could be achieved in the reduction process. A large number of electron rich sites with a reducing agent are capable of controlling the metal particle size and thereby highly dispersed metal/TiO_2 is produced.[20] Another advantageous aspect of hydrazine being used as a reducing agent is that high purity samples are obtained by this technique, since water and N_2 are produced as by-products during the heating process.[20] The physicochemical analysis of mesoporous TiO_2 and various metal incorporated TiO_2 nanocomposites was carried out and some relevant characteristics are compared in Table 1.

Table 1 A comparison of the physicochemical characteristics and photocatalytic hydrogen production rate of mesoporous TiO_2, Cu/TiO_2, Ag/TiO_2 and Ag–Cu/TiO_2 photocatalysts

Photocatalyst	Crystallite size/nm[a]	H_2 yield (mmol h^{-1} g^{-1})[b] (AQY)[b]
TiO_2	8.2	0.16 (0.06 × 10^{-2})
TiAg-1(1 wt% Ag/TiO_2)	7.8	4.59 (1.85× 10^{-2})
TiCu-0.5(0.5 wt% Cu/TiO_2)	13.1	2.08 (0.83 × 10^{-2})
TiCu-1(1 wt% Cu/TiO_2)	14.2	1.90 (0.76 × 10^{-2})
TiCu-5(5 wt% Cu/TiO_2)	13.8	1.10 (0.44 × 10^{-2})
TiAgCu-1 (0.75 wt% Ag + 0.25 wt% Cu/TiO_2)	13.0	6.67 (2.69 × 10^{-2})
TiAgCu-2(0.5 wt% Ag + 0.5 wt% Cu/TiO_2)	14.0	5.05 (2.03× 10^{-2})
TiAgCu-3 (0.25 wt% Ag + 0.75 wt% Cu/TiO_2)	12.2	5.95 (2.40 × 10^{-2})

[a] Obtained from the Scherrer equation using the anatase (101) feature. [b] Hydrogen evolution rate and apparent quantum yield (AQY) are measured for the photocatalyst in thin-film form.

The XRD patterns of TiO_2 and the metal integrated TiO_2 nanocomposites are shown in Fig. 1. The crystallite size of the different composites was determined by the Debye–Scherrer equation[24] using the (101) feature of TiO_2 in the XRD pattern and found to be in the range of 8–14 nm (Table 1). Although well-defined crystalline peaks are observed in all cases, the

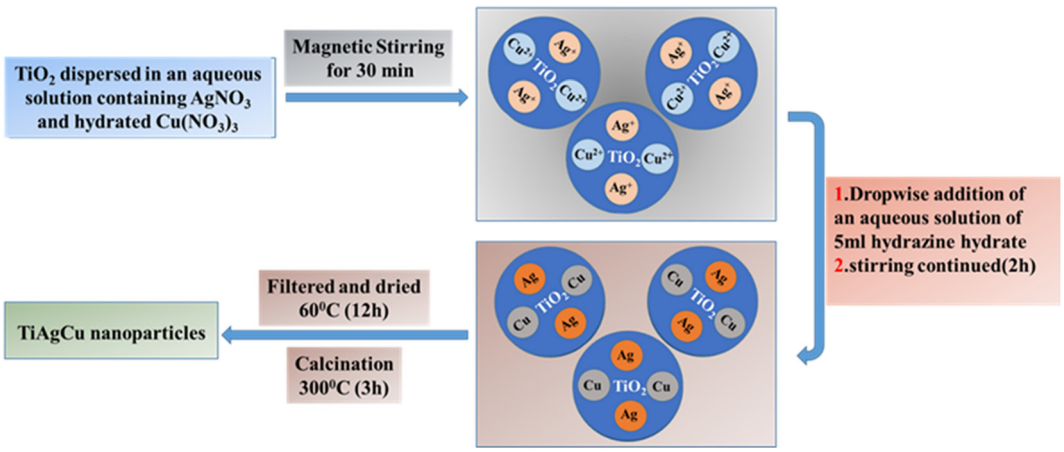

Scheme 1 Schematic illustration of the synthesis of mesoporous Ag–Cu/TiO_2 nanocomposites.

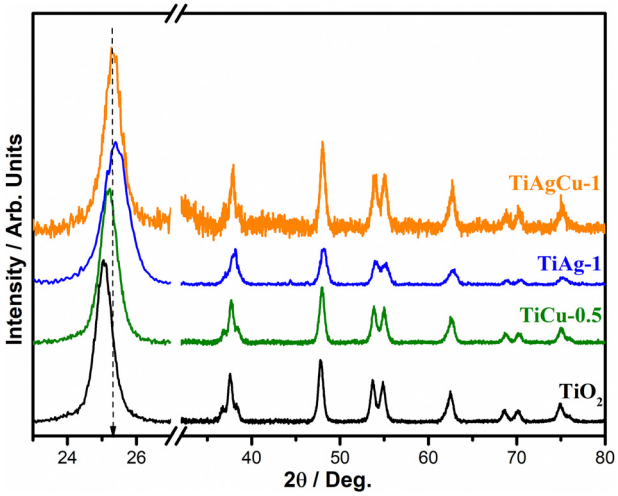

Fig. 1 Wide angle XRD patterns of mesoporous TiO_2, Ag/TiO_2 (TiAg-1), Cu/TiO_2 (TiCu-0.5) and TiAgCu-1 nanocomposites. A significant shift and broadening of the (101) diffraction feature is observed with TiAg-1 and TiAgCu-1. All the diffraction features are attributed to the anatase phase of TiO_2.

broadened feature of the XRD patterns indicates that the materials are nanocrystalline in nature. The TiO_2, TiCu-0.5, TiAg-1 and TiAgCu-1 composites exhibit diffraction features that are characteristic of the anatase phase of TiO_2 (JCPDS no. 21-1272).[13,21,22]

No diffraction peaks characteristic of metallic phases of Ag and Cu, and/or copper oxide phases are observed in any of the photocatalysts.[23] Generally, a high dispersion of small metal particles integrated with the TiO_2 framework is the possible reason that metal diffraction features were not observed.[5,15] Interestingly, a significant shift in (101) diffraction feature was observed with TiAg-1 (0.18^0) along with broadening; however, with Cu/TiO_2 and/or TiAgCu-1 only a peak shift was observed, but without broadening. First of all, this indicates a difference in interaction between TiO_2 with Ag, and Cu or Cu + Ag. The metal nanoparticles in the Ag–Cu loaded TiO_2 composite may alter the surface structure of TiO_2 and also may occupy the defect sites in TiO_2, which leads to a slight shift in the XRD peak as previously reported.[5,25] While the broadening with Ag/TiO_2 indicates a decrease in crystallite size, it is the opposite with Cu and Cu + Ag. The shift observed in XRD is predominantly with the (101) facet of anatase TiO_2, which is abundantly available on the titania surface; no other crystallographic facet shows observable shift, after metal Ag–Cu integration. It may also be noted that Ag loading alone does not affect the crystallite size significantly; the observed crystallite size for TiO_2 and TiAg-1 is in the range of 8 ± 0.5 nm (Table 1). Nonetheless, the crystallite size of all the Cu/TiO_2 and $Ag–Cu/TiO_2$ nanocomposites was found to be 13.2 ± 2 nm, indicating the influence of Cu or Cu + Ag on the TiO_2 crystallite size. It is likely that smaller Cu-size (Cu^0–0.128 nm; Cu^{2+}–0.087 nm) enhances its integration better with TiO_2 than the relatively bigger size silver (Ag^0–0.144 nm; Ag^+–0.129 nm); in particular, the precursor ions (Cu^{2+} and Ag^+) employed in the synthesis also suggest that a large difference in diameter and di-positive charge on copper supports its integration with electron-rich vacancy sites of titania better than silver. Nonetheless, why the crystallite size increases with Cu-containing catalysts is a question. The integration of silver and/or copper with TiO_2 generally occurs through oxygen vacancy sites, which leads to a better integration of metal NPs over the TiO_2 surface; this also leads to electronic integration of the metal with TiO_2, which is evident from the XRD results.[25]

FESEM and TEM images of TiO_2 and metal integrated TiO_2 nanocomposites are shown in Fig. S1 (ESI†) and Fig. 2, respectively. The uniform contrast observed in the TEM images indicates that the metal nanoparticles seem to be highly dispersed.[26] A porous network of particle assembly observed in Fig. 2a–c indicates the possibility of facile diffusion of the reactants and products to the reaction sites; this is also likely to help avoid mass-transfer limitations. TEM and HRTEM images demonstrate that the majority of the particles are in the size

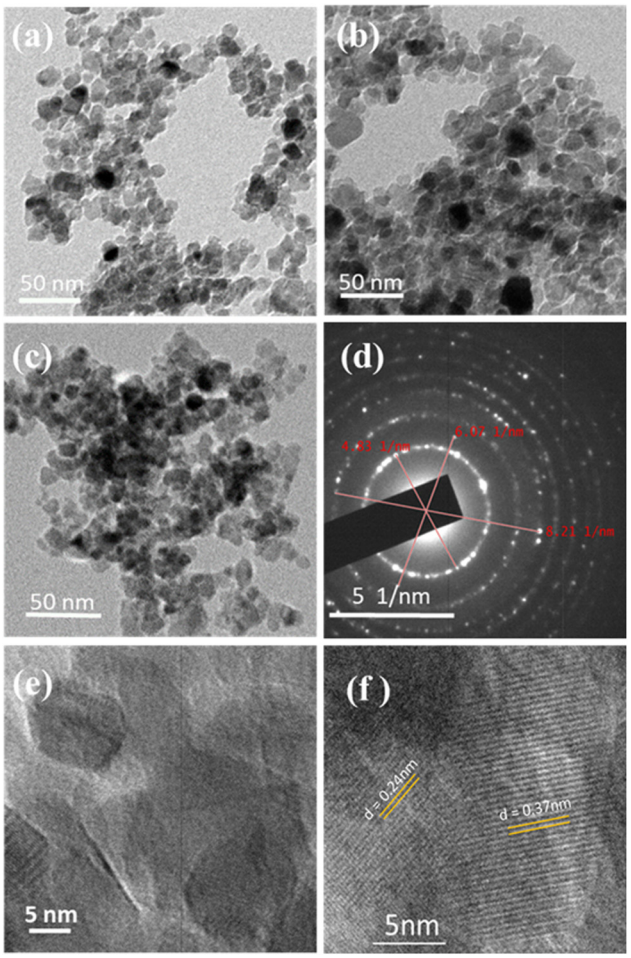

Fig. 2 TEM images of (a) TiO_2, (b) TiCu-1, and (c) TiAg-1; (d) SAED pattern of TiAgCu-1, and HRTEM images of (e) TiAgCu-1 and (f) the lattice fringe spacing in TiAgCu-1. Ag and Cu integration on TiO_2 and the formation of a metal–semiconductor Schottky junction between Ag/Cu and TiO_2 is evident from the *d*-values (0.24 nm for Ag/Cu alloy formation and 0.37 for TiO_2) observed in the HRTEM image in (f).

range of 13 ± 3 nm, and apparently the crystallite and particle sizes are the same, especially for Cu and/or Cu + Ag integrated TiO_2. The SAED pattern of TiAgCu-1 shown in Fig. 2d is composed of well-defined circular rings with bright spots, which is characteristic of the TiO_2 anatase phase. The HRTEM images of TiAgCu-1 in Fig. 2e and f illustrate that the photocatalyst is highly nanocrystalline in nature with a homogeneous distribution of metal nanoparticles on the surface of TiO_2 and a number of metal–semiconductor Schottky junctions are observed. The HRTEM image of TiAgCu-1 shown in Fig. 2f reveals the (101) facet of TiO_2 (0.35 nm); another interlayer *d*-spacing of 0.24 nm could correspond to Ag–Cu bimetal. It is to be noted that no isolated Ag and/or Cu particles were observed in the HRTEM of TiAgCu-1, which supports the formation of Ag–Cu alloy and the Schottky junctions[27] observed between Cu–Ag alloy nanoparticles and the TiO_2(101) facet.[5] Furthermore, the Ag(111) interlayer *d*-spacing is reported to be between 0.23 and 0.236 nm;[19] however, the significantly higher *d*-spacing (0.24 nm) observed is attributed to Ag–Cu alloy.[28]

To evaluate the dispersion of Cu and Ag on TiO_2, chemical mapping was carried out with HRTEM-EDS, and the distribution of all four elements, namely Ti, O, Ag and Cu, is shown in Fig. S2 (ESI†). A uniform distribution of very small Ag and Cu particles in Fig. S2 and Table S6 in the ESI† highlights a fine distribution all over the titania surface. Such fine distribution also ensures plenty of Schottky junctions[29] with titania particles and is likely to enhance the charge separation.

Absorption spectral studies of the photocatalyst nanocomposites

UV-visible absorption spectra of TiO_2 and all metal incorporated TiO_2 nanocomposites are shown in Fig. 3. Bare TiO_2 exhibits a strong absorption below 400 nm (UV region) due to the band gap excitation of the anatase phase of TiO_2. However, metal integrated TiO_2 nanocomposites exhibited a prominent light absorption in the visible region due to the strong SPR effect exhibited by both Cu and Ag.[11] Besides the SPR effect of the Ag (420 nm) and Cu (~600 nm) nanoparticles, the strong interaction between TiO_2 and metal nanoparticles may further enhance the optical absorption in the visible region.[30] The colour change observed for the photocatalyst from white for TiO_2 to green or grey tint for Cu/TiO_2 or Ag/TiO_2, respectively, and greyish green for Ag–Cu/TiO_2 (see inset in Fig. 3) indicates that the visible light absorption is due to metal integration with TiO_2. The efficiency of light absorption is extended to the visible region, after metal nanoparticles are integrated with the TiO_2 matrix. Metal nanoparticles and TiO_2 may have different Fermi levels, as independent entities; however, after their integration, especially after electronic integration, the Fermi level of the composite would shift closer to that of TiO_2. This is expected to increase the charge separation at the Schottky junctions.[5,16]

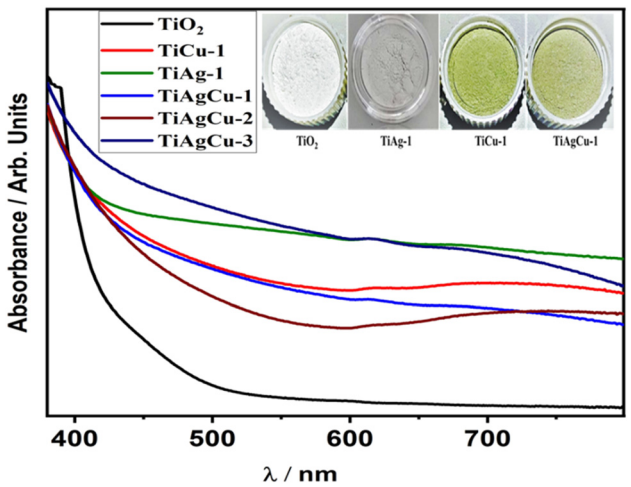

Fig. 3 UV Visible absorption spectra of mesoporous TiO_2 and representative samples of metal integrated TiO_2 nanocomposites.

Electrochemical studies of the photocatalyst nanocomposites

Electrochemical impedance spectroscopy (EIS) plots were recorded to investigate the kinetics and electron transport behaviour of various electrodes prepared using TiO_2, TiAg-1, TiCu-1, and TiAgCu-1. The Nyquist plot for the representative samples is shown in Fig. 4a and it was analysed by fitting with an equivalent circuit model R(CR), as shown in the inset in Fig. 4a. The impedance parameters (R_S, C_{dl}, and R_{ct} corresponds to solution resistance, double layer capacitance, and charge transfer resistance respectively) obtained from the equivalent circuit after fitting are given in Table S1 (ESI†).[31,32] It is evident from the fitting parameters (Table S1, ESI†) that the R_{ct} values of TiO_2, TiCu-1, TiAg-1, and TiAgCu-1 are 329.0, 142.70, 99.21 and 27.69 Ω, respectively. The above decreasing trend in the R_{ct} values suggests that the electron transfer rate increases in the order TiO_2 < TiCu-1 < TiAg-1 < TiAgCu-1.[33] Thus, TiAgCu-1 having the lowest R_{ct} value shows the maximum charge separation and electron transfer rate. The C_{dl} values of different photocatalysts decrease in the order: TiAgCu-1 > TiAg-1 > TiCu-1 > TiO_2. The highest C_{dl} value of TiAgCu-1 implies that the material has high active surface area and this is due to its surface heterogeneity and superior electron transport characteristics. The high active surface area provides a large number of active sites for efficient water splitting reaction.[34] Among the different photocatalysts, the radius of the arc in the Nyquist plots is in the order TiO_2 > TiCu-1 > TiAg-1 > TiAgCu-1. A smaller impedance arc radius in the Nyquist plot indicates an efficient separation and migration of photogenerated charge carriers, and hence the lowest charge transfer resistance and high charge carrier mobility.[28]

TiAgCu-1 exhibits the smallest impedance arc radius and the highest C_{dl} value, suggesting that it has the least resistance for the dispersion of charge carriers and the highest interfacial electron transfer rate among the composites studied.[32,33] High electron transfer rate, efficient charge separation and increased active surface area with a large number of electro active components are factors that help to achieve improved photocatalytic performance.

Fig. 4b displays the photocurrent responses of representative samples performed in light on/off cycles in order to

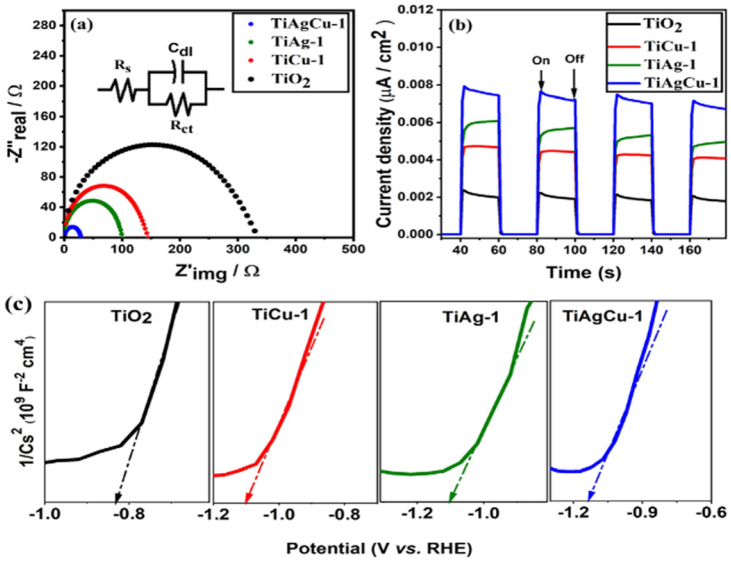

Fig. 4 (a) Nyquist plots, (b) transient photocurrent responses under light illumination conditions, and (c) Mott–Schottky plot of TiO_2, TiAg-1, TiCu-1, and TiAgCu-1. The electrochemical experiments were carried out in 0.5 M Na_2SO_4 (pH = 7.5) at a potential of 1.23 V (*vs.* NHE).

determine the charge density and charge separation efficiency of the photocatalysts. High and instant photocurrent response indicates an efficient dispersion of charge carriers and the separation of electrons and holes, which are essential qualities to produce photocurrent.[28,35] The photocurrent density observed for various photocatalysts in the present study follows the order: TiAgCu-1 > TiAg-1 > TiCu-1 > TiO_2 and it is clear evidence of the SPR effect exhibited by Cu/Ag nanoparticles. Integration of metallic particles with TiO_2 increases the photocurrent density, implying that the metal species in the (Ag,Cu)/TiO_2 nanocomposite increases the charge carrier separation and migration efficiency. Although 1 wt% of metal is present in TiAg-1 and TiCu-1, the atom percent is higher with the latter due to lower atomic weight of Cu (63.546) than Ag (107.868); nonetheless, TiAg-1 exhibits significantly higher photocurrent density than TiCu-1 indicating a better integration of Ag due to its smaller TiO_2 crystallite size. The very low R_{ct} value and highest photocurrent response of TiAgCu-1 demonstrates that the synergetic interaction between Ag and Cu in the composite catalyst has a remarkable ability to improve the separation and transfer of photo-generated charge carriers at the composite interface. Although the individual metal content in TiAgCu-1 (0.75 wt% Ag and 0.25 wt% Cu) is lower than that of either TiAg-1 or TiCu-1, the current density observed is higher and it directly indicates the possibility of the plasmon induced resonance energy transfer (PIRET) effect. PIRET arises through a non-radiative energy transfer process from the dipole of plasmonic metal NPs to the dipole of the excited semiconductor in a restricted area around it; indeed it is preferred, if plasmonic metal NPs and TiO_2 are integrated, which enhances the energy transfer. It is very likely that direct electron transfer as well as some PIRET effect occurs in the present system. The positive slopes of the Mott–Schottky (MS) plots displayed in Fig. 4c illustrate the typical n-type semiconductor characteristics of the materials.[9] The conduction band positions of TiO_2, TiCu-1, TiAg-1, and TiAgCu-1 calculated from the MS plots are −0.88, −1.10, −1.12, −1.13 eV, respectively. Shifting of the conduction band position of the metal integrated TiO_2 nanocomposites towards a more negative value compared to the conduction band position of pure TiO_2 indicates that the metal-integrated TiO_2 in the present study is highly efficient for the water reduction process.

XPS studies of the photocatalyst nanocomposites

The photoelectron spectra of Ag 3d, and Cu 2p core levels and Auger electron spectra of Cu $L_3M_{45}M_{45}$ are shown in Fig. 5a–c, respectively. The XPS results derived from various peak components for Cu/TiO_2 and Ag–Cu/TiO_2 nanocomposites are summarized in Table S2 in the ESI.† The Ti 2p core level features of all photocatalyst nanocomposites (results not shown) exhibit identical features with spin–orbit components at BE of 458.8 ± 0.2 and 464.6 ± 0.2 eV corresponding to Ti $2p_{3/2}$ and $2p_{1/2}$ peaks, respectively. The spin orbit separation (5.7 eV) and the BE values are characteristic for the Ti^{4+} state.[36] The Ag 3d core level spectra of the Ag–Cu/TiO_2 nanocomposites are displayed in Fig. 5a, which shows Ag $3d_{5/2}$ and $3d_{3/2}$ core level peaks at 367.3 ± 0.1 and 373.3 ± 0.1 eV, respectively with a spin–orbit separation of 6 eV; metallic Ag $3d_{5/2}$ appears at 368 eV, and the present set of lower BEs indicates that Ag could be in a significantly different electronic state due to integration with TiO_2 and possible electron transfer to Ag from the latter.[37] Lower BE shift of the Ag 3d peaks suggests that a strong electronic interaction between TiO_2 and Ag nanoparticles exists through the formation of a Schottky junction.[1] The Cu $2p_{3/2}$ photoelectron spectra of the Cu/TiO_2 and Ag–Cu/TiO_2 photocatalysts are presented in Fig. 5b showing Cu $2p_{3/2}$ core level features at BE values of around 932.7 ± 0.1 eV. Very minor satellite features are observed between 940 and 947 eV

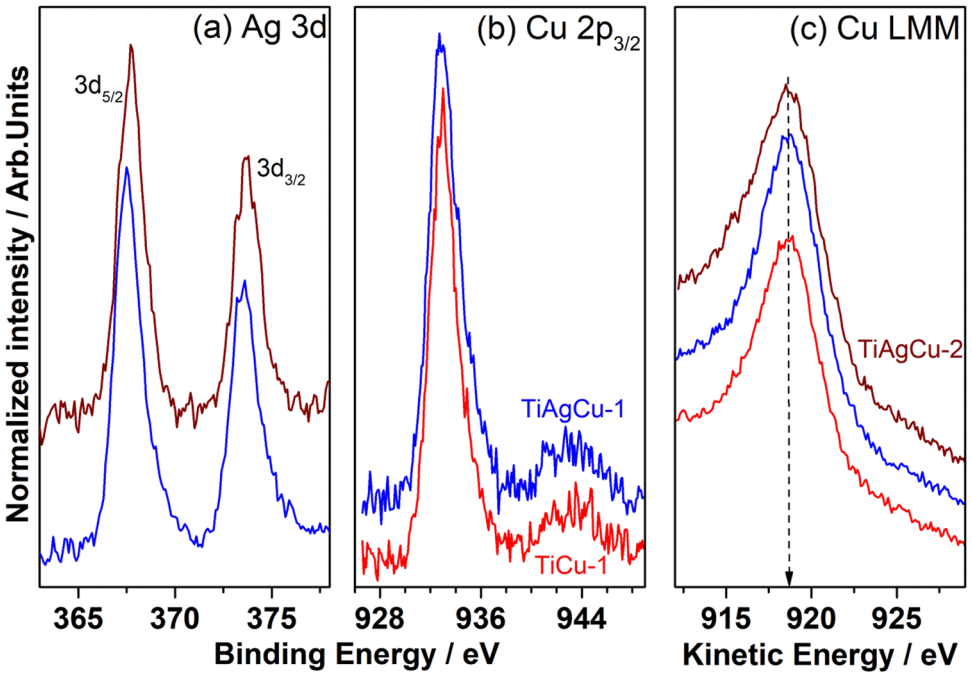

Fig. 5 XPS core level spectra recorded for (a) Ag 3d and (b) Cu $2p_{3/2}$ core levels, and (c) X-ray initiated Auger electron spectra recorded for Cu-$L_3M_{45}M_{45}$ transition for TiCu-1, TiAgCu-1 and TiAgCu-2 nanocomposites. Different colours were used for different compositions, namely, TiCu-1 (red), TiAgCu-1 (blue), and TiAgCu-2 (brown).

indicating some inevitable surface oxidation, due to exposure to atmospheric components. However, the Cu $2p_{3/2}$ feature observed at 932.7 eV could be due to either metallic Cu or Cu^+ species, and it cannot be distinguished by core level XPS.

A further confirmation of the oxidation states of Cu species in the Cu/TiO_2 and Ag–Cu/TiO_2 nanocomposites was obtained by analysis of the Cu LMM Auger analysis. As shown in Fig. 5c it exhibits a single component at kinetic energy (KE) value 918.7 ± 0.2 eV, which is characteristic of metallic Cu.[5,38,39] The high intensity peak at 918.7 eV underscores the predominant presence of metallic Cu. It is also noted that Cu^+ and Cu^{2+} appear at a KE of 916.8 and 918.0 eV, respectively.[38,39] The modified Auger parameter (α) (Table S2 in ESI†) is a valid indicator for understanding the Cu binding state and to confirm the presence of metallic Cu in all nanocomposites evaluated.[39] The modified Auger parameters calculated are 1851.4 ± 0.2 eV, indicating the larger contribution of Cu^0 on all the Cu containing samples.[38] Metallic Cu observed with all Cu-containing catalysts fully supports the earlier observations of Schottky junctions and visible light absorption. Different factors such as the input amount of Cu, ratio of Cu to Ag, and Ag–Cu alloy formation could contribute to the percentage of metallic Cu in the catalyst.

Photocatalytic activity evaluation of Ag/TiO_2, Cu/TiO_2 and Ag–Cu/TiO_2 nanocomposites

The photocatalytic hydrogen evolution activity of both powder and thin film forms of all nanocomposite materials were evaluated using an optimized amount of 1 mg catalyst (see Tables S3 and S4 for details, ESI†) and the rates of hydrogen evolution obtained for the thin-film forms are compared in Table 1 and Fig. 6. As evident in Fig. 6, a very low yield of H_2 production (0.16 mmol h^{-1} g^{-1}) was observed for the TiO_2 thin-film; however, it increased after integration of Cu, Ag or Cu + Ag with TiO_2. Among all Cu/TiO_2 photocatalysts, TiCu-0.5 showed the highest hydrogen production rate and its activity was about 13 times higher than that of bare TiO_2 under comparable experimental conditions. However, TiCu-1 exhibits a rate very

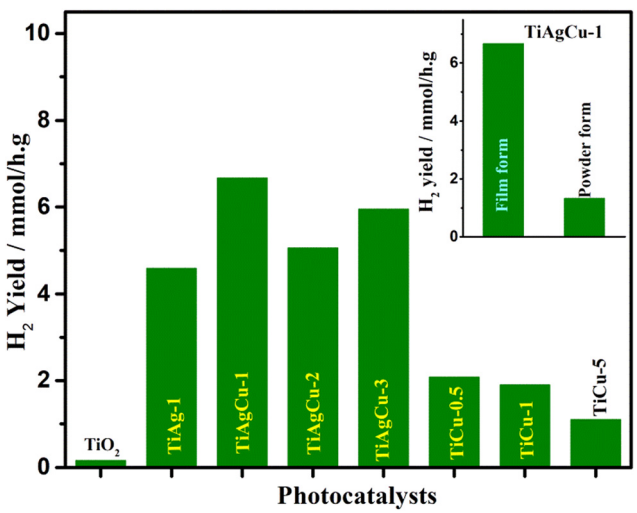

Fig. 6 Photocatalytic H_2 production activity of mesoporous TiO_2, Ag/TiO_2, Cu/TiO_2 and Ag–Cu/TiO_2 nanocomposites, measured in thin film form under direct sunlight. Inset shows a comparison of the solar hydrogen generation activity for the thin film and powder catalysts of TiAgCu-1.

close to that of TiCu-0.5, and within 10% error limit. Interestingly, the H_2 production activity on Ag/TiO_2 was higher than that of the Cu/TiO_2 photocatalysts. For example, the hydrogen production rate of TiAg-1 was 4.59 mmol h^{-1} g^{-1}, which is 2.3 times higher than that of the TiCu-0.5. The Ag–Cu/TiO_2 nanocomposites showed higher activity, irrespective of the three different compositions attempted in this study, than single metal–TiO_2 composites, suggesting that the combination of both Cu and Ag is more effective for solar H_2 production. The H_2 production rates on TiAgCu-1, TiAgCu-2 and TiAgCu-3 in the thin film were 6.67, 5.05 and 5.95 mmol h^{-1} g^{-1}, respectively. Within 10% error limit, the TiAgCu-1 and TiAgCu-3 composites exhibit comparable activity, and a marginally decreased activity with TiAgCu-2. This suggests that the combination of two SPR metals, with possible bimetal/alloy formation, could be helpful to achieve the maximum solar hydrogen generation activity. Among various photocatalysts, TiAgCu-1 (0.75 wt% Ag and 0.25 wt% Cu) resulted in the highest H_2 production rate of 6.67 mmol h^{-1} g^{-1}, which is 42 times higher than that of TiO_2. We also compared the photocatalytic water splitting performance of the selected photocatalysts in both powder and thin-film form under similar experimental conditions, while maintaining the same amount of catalyst (1 mg). As shown in the inset in Fig. 6, the activity of TiAgCu-1 in thin-film form (6.67 mmol h^{-1} g^{-1}) was observed to be 5 times higher than that of the corresponding powder form with the same amount of particulate form of the catalyst measured in suspension. Possible reasons for the enhanced activity of the thin-film include the following: (1) the light absorption in the thin-film (10–12 μm thickness) takes place more efficiently due to larger absorption coefficient and effective utilization of the scattered light through a series of internal scattering and eventual absorption, whereas the majority of the light scatters in particulate suspension form. (2) Light penetration in the thin film is to the full depth of 10 microns, and hence the number of charge carriers generated is also enhanced, (3) The thin film form and the maximum number of catalyst particles being in contact with each other enhance the better utilization of charge carriers for the redox reactions and hence the H_2 generation is also observed to be higher. (4) Photocatalyst in the thin-film form can access the maximum amount of reactants due to its larger exposed surface area and facilitate the reaction kinetics by accelerating the diffusion of photogenerated charges toward the reaction sites.[5] Although the catalyst deposition over the glass plate was not uniform and inhomogeneous, H_2 evolution from the entire area of the film surface under direct sunlight irradiation was evident in our study. A short video is provided in the ESI† (see Video V1, in the ESI†), which displays continuous hydrogen generation from the entire region of the thin-film surface visible to the naked eye, while it is not possible to see any H_2 bubble formation in suspension. The AQY value was calculated for various photocatalysts in thin-film form revealing that the AQY is negligibly small for TiO_2; TiAgCu-1 showed the highest AQY (2.7×10^{-2}%) under direct sunlight (see Table 1). It is worth mentioning that the AQY values of all samples in thin film form were high compared to their powder counterparts due to effective light harvesting.

Time on stream (ToS) dependence of solar H_2 production of TiO_2, TiCu-1, TiAg-1 and Ag–Cu/TiO_2 in thin film form under direct sunlight was carried out to explore the sustainability aspects of the catalysts. The cumulative H_2 yield obtained as a function of irradiation time is displayed in Fig. 7a. Compared to TiO_2, all Ag–Cu/TiO_2 composites show an almost steady and nearly equal (within 10% error) increase in H_2 generation as the irradiation time progresses. For example, TiAgCu-2 and TiAgCu-3 displayed a cumulative hydrogen yield of 25.25 mmol h^{-1} g^{-1} and 29.75 mmol h^{-1} g^{-1}, respectively in 5 h in the ToS study and this is much higher than pure TiO_2 (0.8 mmol g^{-1}), TiCu-1 (9.5 mmol h^{-1} g^{-1}) and TiAg-1 (22.9 mmol h^{-1} g^{-1}). Among the Ag–Cu/TiO_2 nanocomposites, TiAgCu-1 and TiAgCu-3 displayed a steady increase in H_2 yield with the highest and comparable cumulative hydrogen production of 33.35 and 29.75 mmol h^{-1} g^{-1} in 5 h, respectively, underscoring the sustainability of the catalysts.

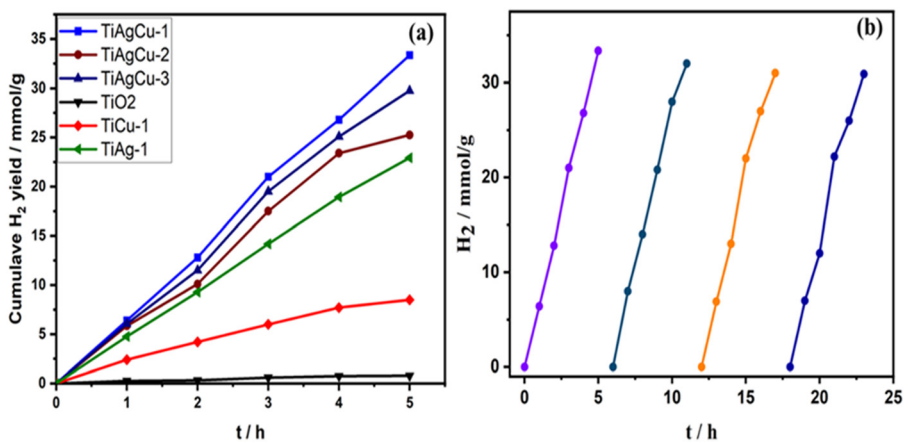

Fig. 7 (a) Time on stream dependence of solar hydrogen production of the mesoporous TiO_2, TiAg-1, TiCu-1 and TiAgCu nanocomposites (in thin film form) from solar hydrogen evolution. (b) Solar hydrogen production as a function of time with repeated cycles of operation for TiAgCu-1 in direct sunlight.

The photostability of the best performing TiAgCu-1 photocatalyst in thin film form was studied by performing the experiments in four repeated cycles, with 5 h per cycle, to ensure the reusability of the catalyst, and the results are displayed in Fig. 7b. The rate of solar hydrogen production was almost the same for all cycles, within 10% error, indicating that the catalyst remains stable under photocatalytic experimental conditions. It is noteworthy that even without employing any binder the catalyst particles were intact on the glass plate during the entire period of the experiments in this study. However, studies with a suitable binder are suggested to evaluate the long-term stability.

The number of reports on H_2 production by water splitting in direct sunlight based on the Ag–Cu/TiO_2 photocatalytic system is very limited in the literature.[15,16] Nonetheless, the H_2 production activity of TiAgCu-1 and other Ag–Cu/TiO_2 in thin-film form in the present study is significantly higher than that of various Ag/TiO_2, Cu/TiO_2 and Ag–Cu/TiO_2 catalysts reported in the literature under comparable experimental conditions. Kotesh Kumar *et al.* reported that 0.5 wt% Ag–2 wt% Cu/TiO_2 synthesized by the wet impregnation method showed a hydrogen production rate of 5.683 mmol g^{-1} h^{-1} under direct sunlight with aqueous methanol.[15] Although this activity is nearly comparable to the activity reported in the current manuscript, a 15% decrease in activity was observed while cycling the catalysts; in addition, ref. 15 also employed a larger amount of metal content in their catalyst. The Ag–Cu bimetal-modified TiO_2 displayed a hydrogen evolution rate of 1.16 mmol h^{-1} g^{-1} with aqueous methanol, under one sun conditions (100 mW cm^{-2}).[16] The photocatalytic H_2 evolution reaction rate observed on Ag–Cu/TiO_2 in the current work is much higher than that of Ag/TiO_2 in thin-film form reported earlier from our laboratory,[2] and various Ag/TiO_2 and Cu/TiO_2 photocatalysts reported in the literature.[18,32,39–41] The hydrogen evolution activity of various Ag/TiO_2, Cu/TiO_2, and Ag–Cu/TiO_2 photocatalysts using methanol as a sacrificial reagent reported in the literature was compared in the Table 2, fully supporting the superior activity associated with the present set of TiAgCu catalysts.

The higher rate of hydrogen evolution activity of the Cu/TiO_2 nanocomposites compared to bare TiO_2 is attributed to the enhanced absorption of visible light due to the SPR effect, and efficient electron transfer from the Cu-SPR state to TiO_2, which limits the combination possibility of the charge carriers.[6] The relatively high photocatalytic activity of Ag/TiO_2 compared to Cu/TiO_2 is attributed to the relatively strong SPR effect by Ag than Cu species, apart from the smaller atom percent of Ag-content.[33] Compared to Cu/TiO_2 and Ag/TiO_2, an unambiguous increase in the solar hydrogen activity was observed with the Ag–Cu/TiO_2 nanocomposites, irrespective of the Ag–Cu composition in the present study. It is also to be noted that the individual metal content is lower than 1 wt% in the Ag–Cu case. The possible reasons that contribute to the higher activity of Ag–Cu/TiO_2 are the following: (1) the combined SPR effect of Ag and Cu facilitates an enhanced absorption of solar light in a wide range of visible light wavelengths. The strong synergistic interaction among Ag and Cu, due to alloy/bimetal formation, and with TiO_2 produces a large number of metal–TiO_2 Schottky junctions as evidenced from the HRTEM images, which facilitates efficient separation of electrons and holes leading to better utilization of charge carriers.[36] (2) Integration of Cu + Ag with TiO_2 leads to the shifting of the Fermi level closer to the CB of TiO_2 and thereby the photo excited electrons in the SPR state are easily transferred to the CB of TiO_2.[13,42] (3) The possible formation of the Ag–Cu alloy on the surface of TiO_2 in the Ag–Cu/TiO_2 nanocomposite film facilitates the maximum absorption of solar light and its effective utilization. (4) An enhanced photocurrent generation as well as solar hydrogen production underscores that the PIRET effect also could be partially contributing to the overall activity. Employing a 455 nm band-pass filter decreased the H_2 generation rate to about 10% value compared to that of AM1.5G (one sun condition) for TiAg-1. Similarly, the 620 nm filter decreased the H_2 generation rate enormously for all Cu-containing photocatalysts. These reference experiments confirm the light absorption through the SPR effect by Ag and Cu, and the solar hydrogen generation activity is predominantly through them.

Among all Ag–Cu/TiO_2 nanocomposites, the highest solar H_2 evolution exhibited by TiAgCu-1 (0.75 wt% Ag and 0.25 wt% Cu) is ascribed to high dispersion of Ag–Cu with relatively high Ag/Cu surface atomic ratio and a heterogeneous distribution of Ag and Cu species, along with other factors discussed earlier. The variation of hydrogen production activity is correlated with the surface atomic ratio calculated from XPS as shown in Fig. 8. TiAgCu-1 showed the highest Ag/Ti (0.04) along with Ag/Cu = 1, indicating nearly equal amount of Ag and Cu present on the surface (Fig. S3, ESI†). Whereas for other samples a relatively Cu rich surface was obtained. The relatively higher surface atomic concentration of metallic species and a heterogeneous distribution of Ag and Cu species on TiAgCu-1 help to form the maximum number of Schottky junctions at the metal–TiO_2

Table 2 Water splitting activity of various Ag–Cu/TiO_2, Ag–TiO_2 and Cu–TiO_2 photocatalysts reported in the literature

No.	Photocatalyst	Reaction conditions	Sacrificial reagent	Activity (μmol h^{-1} g^{-1})	Ref.
1	Ag–Cu with co-loaded TiO_2 H:(Ag–Cu/TiO_2)	AM1.5G one sun condition – 100 mW cm^{-2}	Methanol	1160	16
2	Ag and/or Cu on TiO_2 (anatase/rutile)	Direct solar light	Methanol	5683	15
3	1 wt% Ag/TiO_2(TiAg-1)	Direct sunlight	Methanol	4590	2*a*
4	Ag@TiO_2	300 W xenon lamp	Methanol	531.9	1
5	Cu-TiO_2-P25	Hg-vapour lamp – 315–1100 nm–125 W	Methanol	8.74 μmol H_2/min g	3
6	TiAgCu-1	Direct sunlight	Methanol	6670	Present work

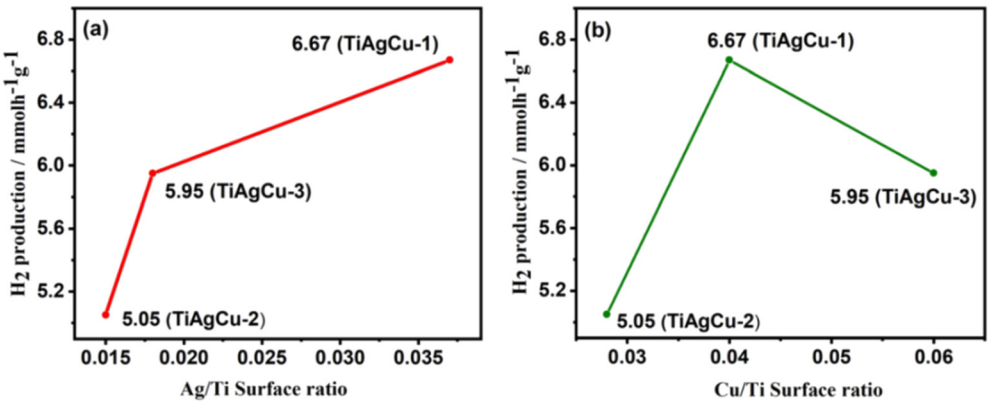

Fig. 8 (a) Variation of rate of hydrogen production with Ag/Ti surface ratio. (b) Variation of rate of hydrogen evolution with Cu/Ti surface ratio.

interface in TiAgCu-1. Equal Cu/Ti and Ag/Ti on TiAgCu-1 and a perfect 1 : 1 Cu : Ag combination observed is attributed to the maximum light harvesting and photocatalytic activity, in spite of different input Cu : Ag ratio. This also supports an Ag–Cu bimetal or alloy formation in the present work.

Mechanism of photocatalytic H_2 production

Based on the experimental and characterization studies on the present catalyst system and various literature studies,[43–48] a plausible mechanism of photocatalytic hydrogen evolution on Ag–Cu/TiO_2 nanocomposites is suggested and is depicted in Fig. 9. When TiO_2 is exposed to solar irradiation, electrons are excited from its VB to the CB leaving the holes in the VB. The photocatalytic activity of the metal integrated TiO_2 nanocomposites carried out under visible light (>420 nm) revealed that the H_2 production rate decreased in all cases compared to direct sunlight (Table S5 in the ESI†). For example, the H_2 production rate on TiAgCu-1 decreased to 72% (4.80 mmol h^{-1} g^{-1}) with respect to direct sunlight (6.67 mmol h^{-1} g^{-1}). 4–5% of UV

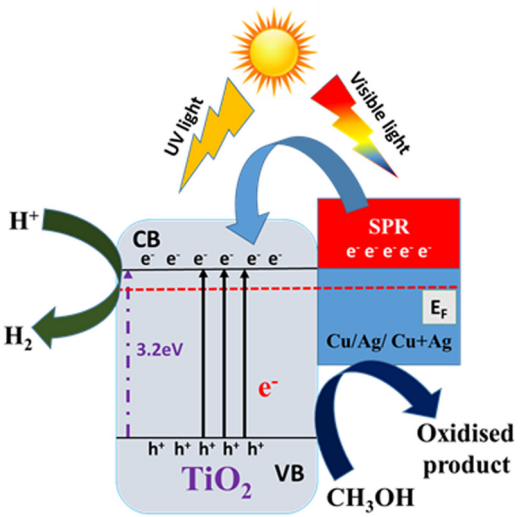

Fig. 9 A schematic illustration of the possible mechanism for SPR-induced electron transfer and co-catalytic activity during photocatalytic reaction of the Ag–Cu/TiO_2 nanocomposite.

available in sunlight also contributes significantly to the activity.[4] Nonetheless, this observation confirms the origin of predominant activity from visible light absorption, which is due to the AgCu alloy. The concurrent SPR effect of the Ag and Cu nanoparticles and enhanced charge density and charge separation efficiency as evidenced from the photocurrent measurements enhances the visible light absorption capacity and transfers more electrons into the CB of TiO_2. As indicated earlier, the PIRET effect also enhances light absorption in the TiO_2 lattice and increases the electron excitation into the CB of TiO_2. Additionally, the high local electronic field increases the energy of trapped electrons and enables them to readily interact with the electron acceptors.[32] The lowest R_{ct} value of TiAgCu-1 evidenced from EIS analysis supports this observation.

Thus the charge carriers are efficiently separated and the electrons concentrated at the metallic surface and CB of TiO_2 are beneficial for enhancing the solar H_2 generation activity. At the same time, the sacrificial agent methanol acts as a hole scavenger, which undergoes oxidation by utilizing holes from the VB of TiO_2 to form CO_2. The interaction between different metals in a bimetallic system can lead to synergistic effects, where the properties of the combined system are different from the sum of its individual components. Indeed, the Ag 4d[37] and Cu 3d[39] bands appear at the same energy in photoelectron spectral studies, supporting the synergetic interaction too. This synergistic effect can enhance the SPR response, making the CuAg system more efficient in interacting with light. Thus, the presence of Ag + Cu nanoparticles at an optimum ratio on the catalyst surface of TiAgCu-1 makes it the best performing nanocomposite with maximum H_2 production rate.

Conclusions

In summary, we report the synthesis of visible light absorbing mesoporous metal integrated TiO_2 nanocomposites (Ag/TiO_2, Cu/TiO_2 and Ag–Cu/TiO_2) through a simple chemical reduction method, and a detailed structure–activity correlation with photocatalytic H_2 evolution activity has been carried out. HRTEM analysis revealed the presence of Schottky junctions at the metal–TiO_2 interface and facilitates the separation of

photogenerated charge carriers. The electrochemical impedance studies revealed that the charge transfer resistance and the charge recombination rate decrease on metal integration with TiO_2 through the formation of an effective metal–TiO_2 heterojunction. The highest transient photocurrent response of TiAgCu-1 observed further supports that the combination of Ag and Cu in the composite catalyst has a remarkable ability to improve the separation and transfer of photo-generated charge carriers at the composite interface.

Photocatalytic H_2 evolution studies on metal integrated TiO_2 nanocomposites revealed that the photocatalyst fabricated in the form of a thin-film showed higher hydrogen production activity than their powder form. The high activity observed with the Ag–Cu/TiO_2 nanocomposites is attributed to factors such as the combined SPR effect of the Ag nanoparticles and co-catalytic activity of Cu, the strong interaction between Ag and Cu and the possible formation of a Ag–Cu alloy, and the shifting of the Fermi level closer to the conduction band of TiO_2. The plausible photocatalytic reaction mechanism is the PIRET and regular light-induced electron excitation of TiO_2 and further promoted by the metal nanoparticles (Cu/Ag/Cu + Ag), which are subsequently utilized for the reduction of H^+ ions to H_2.

Author contributions

This manuscript was written through contributions from all authors. All authors have given approval to the final version of the manuscript.

Conflicts of interest

There are no conflicts to declare.

Acknowledgements

S. R. thanks UGC for the research fellowship. S. M. S. gratefully acknowledges DST, New Delhi, for the facility support under the DST-FIST programme in St. John's College, Anchal, Kerala, India.

References

1 M. Shang, H. Hou, F. Gao, L. Wang and W. Yang, *RSC Adv.*, 2017, **7**, 30051–30059.
2 (*a*) S. S. Mani, S. Rajendran, N. Nalajala, T. Mathew and C. S. Gopinath, *Energy Technol.*, 2022, **10**, 1–12; (*b*) A. A. Melvin, K. Illath, T. Das, T. Raja, S. Bhattacharyyaand and C. S. Gopinath, *Nanoscale*, 2017, **7**, 13477–13488.
3 L. Clarizia, G. Vitiello, G. Luciani, I. Di Somma, R. Andreozzi and R. Marotta, *Appl. Catal., A*, 2016, **518**, 142–149.
4 H. Bajpai, K. K. Patra, R. Ranjan, N. Nalajala, K. P. Reddy and C. S. Gopinath, *ACS Appl. Mater. Interfaces*, 2020, **12**, 30420–30430.
5 B. Tudu, N. Nalajala, P. Saikia and C. S. Gopinath, *Sol. RRL*, 2020, **4**, 1900557.
6 P. Gomathisankar, T. Noda, H. Katsumata, T. Suzuki and S. Kaneco, *Front. Chem. Sci. Eng.*, 2014, **8**, 197–202.
7 W. Fan, Q. Zhang and Y. Wang, *Phys. Chem. Chem. Phys.*, 2013, **15**, 2632–2649.
8 (*a*) P. A. Gross, S. N. Pronkin, T. Cottineau, N. Keller, V. Keller and E. R. Savinova, *Catal. Today*, 2012, **189**, 93–100; (*b*) P. A. Bharad, K. Sivaranjani and C. S. Gopinath, *Nanoscale*, 2015, **7**, 11206–11215.
9 H. Meng, X. Li, X. Zhang, Y. Liu, Y. Xu, Y. Han and J. Xu, *Dalton Trans.*, 2015, **44**, 19948–19955.
10 M. Z. Ge, C. Y. Cao, S. H. Li, Y. X. Tang, L. N. Wang, N. Qi, J. Y. Huang, K. Q. Zhang, S. S. Al-Deyab and Y. K. Lai, *Nanoscale*, 2016, **8**, 5226–5234.
11 F. Wu, X. Hu, J. Fan, E. Liu, T. Sun, T. Sun, L. Kang, W. Hou, C. Zhu and H. Liu, *Plasmonics*, 2013, **8**, 501–508.
12 C. Ligon, K. Latimer, Z. D. Hood, S. Pitigala, K. D. Gilroy and K. Senevirathne, *RSC Adv.*, 2018, **8**, 32865–32876.
13 N. L. Reddy, S. Kumar, V. Krishnan, M. Sathish and M. V. Shankar, *J. Catal.*, 2017, **350**, 226–239.
14 I. Mondal, S. Gonuguntla and U. Pal, *J. Phys. Chem. C*, 2019, **123**, 26073–26081.
15 M. K. Kumar, K. Bhavani, G. Naresh, B. Srinivas and A. Venugopal, *Appl. Catal., B*, 2016, **199**, 282–291.
16 T. Wang, Y. Yang, S. Lim, C. Chiang, J. Lim, Y. Lin, C. Peng, M. Lin and Y. Lin, *Catal. Today*, 2022, **388**, 79–86.
17 M. Xi, X. Guo, X. Feng, L. Qin, S. Z. Kang and X. Li, *Catal. Lett.*, 2020, **150**, 1368–1372.
18 (*a*) N. Nalajala, K. K. Patra, P. A. Bharad and C. S. Gopinath, *RSC Adv.*, 2019, **9**, 6094–6100; (*b*) C. S. Gopinath and N. Nalajala, *J. Mater. Chem. A*, 2021, **9**, 1353–1371.
19 K. K. Patra and C. S. Gopinath, *ChemCatChem*, 2016, **8**, 3294–3311.
20 J. P. Chen and L. L. Lim, *Chemosphere*, 2002, **49**, 363–370.
21 K. Sivaranjani, S. Agarkar, S. B. Ogale and C. S. Gopinath, *J. Phys. Chem. C*, 2012, **116**, 2581–2587.
22 M. Gao, P. K. N. Connor and G. W. Ho, *Energy Environ. Sci.*, 2016, **9**, 3151–3160.
23 M. M. Hasan and N. K. Allam, *RSC Adv.*, 2018, **8**, 37219–37228.
24 P. Devaraji, N. K. Sathu and C. S. Gopinath, *ACS Catal.*, 2014, **4**, 2844–2853.
25 J. Zhou, G. Tian, Y. Chen, J. Q. Wang, X. Cao, Y. Shi, K. Pan and H. Fu, *Dalton Trans.*, 2013, **42**, 11242–11251.
26 I. Chamorro-Mena, N. Linares and J. García-Martínez, *Dalton Trans.*, 2023, **52**, 13190–13198.
27 X. Li, L. Chen, J. Wang, J. Zhang, C. Zhao, H. Lin, Y. Wu and Y. He, *J. Colloid Interface Sci.*, 2022, **618**, 362–374.
28 P. Babu and B. Naik, *Inorg. Chem.*, 2020, **59**, 10824–10834.
29 M. R. Khan, T. W. Chuan, A. Yousuf, M. N. K. Chowdhurya and C. K. Cheng, *Catal. Sci. Technol.*, 2015, **5**, 2522–2531.
30 S. Asadzadeh-khaneghah, A. Habibi-yangjeh, D. Seifzadeh and H. Chand, *Colloids Surf., A*, 2021, **617**, 126424.
31 M. Yu, H. Sun, X. Huang and Y. Yan, *Nanoscale Res. Lett.*, 2020, **135**, 1–8.
32 E. Liu, L. Kang, Y. Yang, T. Sun, X. Hu, C. Zhu, H. Liu, Q. Wang, X. Li and J. Fan, *Nanotechnology*, 2014, **25**, 165401.
33 (*a*) B. Tudu, N. Nalajala, K. Reddy, P. Saikia and C. S. Gopinath, *ACS Appl. Mater. Interfaces*, 2019, **11**, 32869–32878;

(*b*) B. Tudu, N. Nalajala, K. Reddy, P. Saikia and C. S. Gopinath, *ACS Sustainable Chem. Eng.*, 2021, **9**, 13915–13925.
34 A. A. Krishnan, M. A. Aneesh Kumar, R. B. Nair, R. Sivaraj, A. Lamiya, P. K. Jishnu, S. Kurian, T. Mathew and P. S. Arun, *New J. Chem.*, 2022, **46**, 22256–22267.
35 S. Kumar, N. Lakshmana, A. Kumar, M. Venkatakrishnan and V. Krishnan, *Int. J. Hydrogen Energy*, 2017, **43**, 1–15.
36 P. Zhang, T. Song, T. Wang and H. Zeng, *RSC Adv.*, 2017, **7**, 17873–17881.
37 M. K. Ghosalya, K. P. Reddy, R. Jain, K. Roy and C. S. Gopinath, *J. Chem. Sci.*, 2018, **130**, 1–11.
38 T. Mathew, N. R. Shiju, K. Sreekumar, B. S. Rao and C. S. Gopinath, *J. Catal.*, 2002, **417**, 405–417.
39 K. Roy and C. S. Gopinath, *Anal. Chem.*, 2014, **86**, 3683–3687.
40 Y. Yu, Y. Chen and Z. Cheng, *Int. J. Hydrogen Energy*, 2015, **40**, 15994–16000.
41 M. Jung, J. Scott, Y. H. Ng, Y. Jiang and R. Amal, *Int. J. Hydrogen Energy*, 2014, **39**, 12499–12506.
42 H. Sun, S. Zeng, Q. He, P. She, K. Xu and Z. Liu, *Dalton Trans.*, 2017, **46**, 3887–3894.
43 K. K. Patra, P. A. Bharad, V. Jain and C. S. Gopinath, *J. Mater. Chem. A*, 2019, **7**, 3179–3189.
44 J. B. Priebe, J. Radnik, C. Kreyenschulte, A. J. J. Lennox and H. Junge, *ChemCatChem*, 2017, **9**, 1025–1031.
45 N. Nalajala, K. N. Salgaonkar, I. Chauhan, S. Mekala and C. S. Gopinath, *ACS Appl. Energy Mater.*, 2021, **4**, 13347–13360.
46 M. A. Nadeem, M. Al-Oufi, A. K. Wahab, D. Anjum and H. Idriss, *ChemistrySelect*, 2017, **2**, 2754–2762.
47 (*a*) X. Ren, J. Wang, S. Yuan, C. Zhao, L. Yue, Z. Zeng and Y. He, *Front. Chem. Sci. Eng.*, 2023, **17**, 1949–1961; (*b*) C. Zhao, L. Yue, S. Yuan, X. Ren, Z. Zeng, X. Hu, L. Zhao, Y. Wu and Y. He, *J. Ind. Eng. Chem.*, 2024, **132**, 135–111111.
48 S. Rajendran, S. S. Mani, T. R. Nivedhitha, A. A. Krishnan, P. S. Arun, T. Mathew and C. S. Gopinath, *ACS Appl. Energy Mater.*, 2024, **7**, 104–116.